

Spontaneous rotational symmetry breaking in KTaO_3 interface superconductor

Guanqun Zhang,^{1,*} Lijie Wang,^{1,*} Jinghui Wang,^{2,*} Guangyi Huang,¹ Huanyi Xue,¹ Yueshen Wu,² Yanru Song,^{3,†} Zhenghua An,^{1,4} Jun Li,^{2,‡} Yan Chen,¹ and Wei Li^{1,§}

¹*State Key Laboratory of Surface Physics and Department of Physics, Fudan University, Shanghai 200433, China*

²*School of Physical Science and Technology, ShanghaiTech University, Shanghai 201210, China*

³*Center for Transformative Science, ShanghaiTech University, Shanghai 201210, China*

⁴*Institute for Nanoelectronic Devices and Quantum Computing, Fudan University, Shanghai 200433, China*

(Dated: March 9, 2022)

We report a spontaneous rotational symmetry breaking of the superconductivity at the interface of $\text{YAlO}_3/\text{KTaO}_3$ with superconducting transition temperature of 1.86 K. Both the magnetoresistance and upper critical field under an in-plane field manifest striking asymmetric twofold oscillations deep inside the superconducting state, whereas the anisotropy vanishes in the normal state, demonstrating that it is an intrinsic property of the superconducting phase. We attribute this behavior to the mixed-parity superconducting state with a mixture of *s*-wave and *p*-wave pairing components induced by strong spin-orbit coupling. Our work demonstrates the unconventional character of the pairing interaction in the KTaO_3 interface superconductor and sheds new light on the pairing mechanism of interfacial superconductivity with inversion symmetry breaking.

The study of intriguing interface superconductivity has been a central theme in condensed matter physics in recent years [1], because the presence of inversion symmetry breaking and the interfacial coupling between two constitute materials are expected to promote the strong interplay between electron correlations, providing an ideal platform for unveiling the inherent pairing mechanism of unconventional superconductivity and holding promising potential for the development of superconductor-based devices [2–4]. The prototype interface superconductivity is experimentally observed at the interface of $\text{LaAlO}_3/\text{SrTiO}_3$ with superconducting transition temperature (T_c) of 250 mK [5]. Subsequently, the superconductivity at the interface of $\text{La}_{1.55}\text{Sr}_{0.45}\text{CuO}_4/\text{La}_2\text{CuO}_4$ is also observed [6]. Interestingly, the monolayer FeSe films grown on SrTiO_3 substrates indicate superconductivity above 100 K by compared to their bulk with T_c below 8 K [7–9], suggesting that the electron correlations and the interfacial coupling cooperatively contribute to the remarkable enhancement of superconductivity [10].

Very recently, an unexpected crystalline-orientation dependent superconductivity is experimentally observed at the interface between EuO (or LaAlO_3) and KTaO_3 ($T_c \sim 2$ K) [11–13], which shows near two orders of magnitude enhancement in T_c compared to its three-dimensional counterpart [14]. This indicates that the superconductivity at KTaO_3 interfaces is thought to be an intrinsic interface effect, and the dimensional reduction induced strong electron correlation plays a crucial role in the (111)-oriented KTaO_3 interfaces to prompt the ground state symmetry breaking spontaneously. Notably, an intriguing broken symmetry phase with a strong in-plane anisotropy of the electrical resistance has been observed at the interface of ferromagnetic EuO and KTaO_3 [11]. Theoretically, this symmetry breaking phase in EuO/KTaO_3 is suggested from the

combination effects of the ferromagnetic order in EuO and the strong electron correlation at the interface of EuO/KTaO_3 [15], leading the intrinsic nature of rotational symmetry breaking in KTaO_3 interface superconductor to be elusive.

In this Letter, we carry out an experimental study on nonmagnetic YAlO_3 thin films with a wide-band gap of 7.9 eV grown on the polar $\text{KTaO}_3(111)$ substrates, which is significantly larger than that of LaAlO_3 (5.6 eV) [16], enabling strong confinement potential to restrict the interfacial conducting electrons in a thinner interfacial layer and prompt intriguing quantum behaviors at their interface [17]. Electrical transport measurements on the as-grown films reveal two-dimensional superconductivity with a T_c of 1.86 K and superconducting layer thickness of 4.5 nm. By tuning the in-plane azimuthal angle φ -dependent magnetic field, both the magnetoresistance and upper critical field display pronounced asymmetric twofold oscillations manifested deep inside the superconducting state that vanish in the normal state. These results unambiguously demonstrate that the anisotropy with in-plane rotational symmetry breaking is an intrinsic property of the superconducting phase in $\text{YAlO}_3/\text{KTaO}_3$, and thus, we classify the inversion symmetry breaking KTaO_3 interface superconductor as a mixed-parity unconventional superconductivity with a mixture of *s*-wave and *p*-wave pairing components.

The heterostructures of $\text{YAlO}_3/\text{KTaO}_3$ are prepared by depositing YAlO_3 films on a (111)-oriented KTaO_3 single crystal substrate by pulsed laser deposition (see Supplementary Materials [18]). Atomic force microscopy characterizations show that the surface of KTaO_3 substrates and YAlO_3 films are atomically flat (see Fig. S1 [18]). X-ray diffraction displays the absence of epitaxial peaks of YAlO_3 (see Fig. S2 [18]), suggesting that the YAlO_3 film is not in a well-defined crystalline phase. The microstructure of the interface is

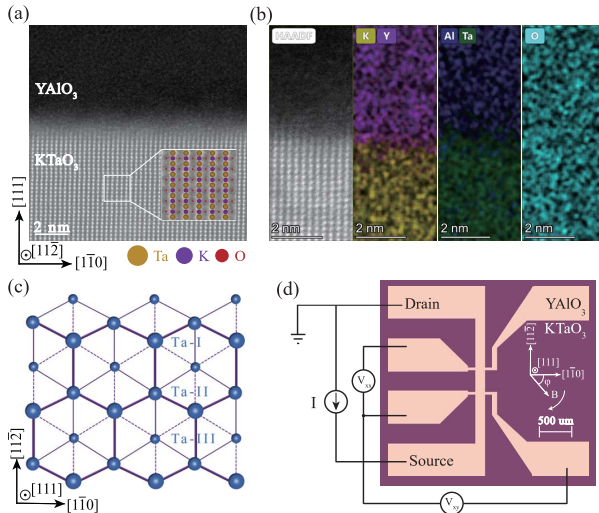


FIG. 1. (a) HAADF-STEM image of YAlO₃/KTaO₃ viewed along the [112] zone axis. The inset shows the enlarged HR-STEM image of KTaO₃ overlaid with atomic configuration (colored). (b) HR-STEM image and the corresponding EDS elemental mapping of interface. (c) Distribution of Ta⁵⁺ ions viewed along the [111] crystal axis of KTaO₃(111) surface. Ta⁵⁺ ions are shown with progressively smaller sizes in the three adjacent (111) planes, which are labeled as Ta-I, Ta-II, and Ta-III, respectively. (d) Hall bar structure on YAlO₃/KTaO₃(111) heterostructure. Here, the φ is defined as the in-plane azimuthal angle between an applied magnetic field and the [110]-axis of the lattice shown in the inset of (d).

further examined by aberration-corrected STEM. From the HAADF-STEM image [see Fig. 1(a)], it can be observed that the amorphous phase YAlO₃ thin film is grown on the KTaO₃(111) substrate. From a larger field of view, the thickness of the YAlO₃ film is about 60 nm. HR-STEM imaging [Fig. 1(a)] and EDS elemental mapping [Fig. 1(b)] demonstrate that the interface of YAlO₃/KTaO₃ is clearly resolved structurally and chemically, suggestive of high-quality growth of the YAlO₃ films on the KTaO₃ substrates.

Fig. 2(a) shows the temperature-dependent sheet resistance R_s on two representative as-grown YAlO₃ thin films (Samples #1 and #2 with growth temperatures of 780 °C and 650 °C, respectively) with the Hall bar structure, schematically illustrated in Fig. 1(d). A typical metallic behavior is visible in a wide temperature range, indicative of the two-dimensional electron gas formed at their interface induced from a combination of the polar KTaO₃ and oxygen vacancies. Through the Hall effect measurements at 5 K, the transverse Hall resistance R_{xy} reveals that the charge carriers in the YAlO₃/KTaO₃ are electrons, and the carrier density is estimated to be $1.45 \times 10^{14} \text{ cm}^{-2}$ and $6.62 \times 10^{13} \text{ cm}^{-2}$ for Samples #1 and #2, respectively. The electron mobility for Samples #1 and #2 is thus evaluated to be $193.6 \text{ cm}^2 \text{V}^{-1} \text{s}^{-1}$ and $159.7 \text{ cm}^2 \text{V}^{-1} \text{s}^{-1}$. These results are highly repro-

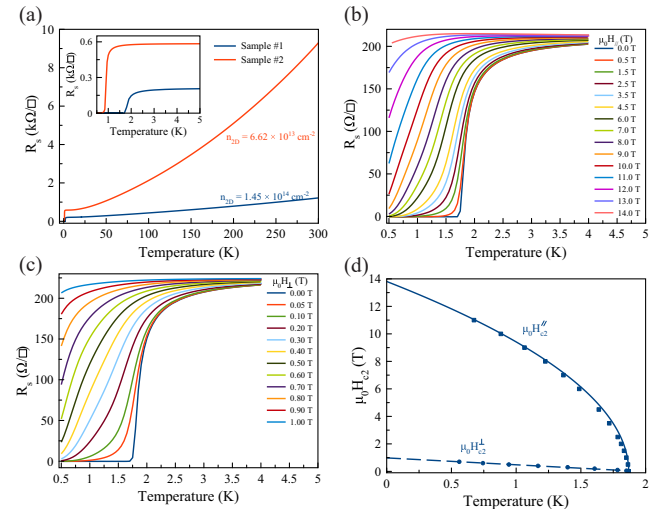


FIG. 2. (a) Electrical resistance (R_s) as a function of temperature ranging from 0.5 mK to 300 K at zero magnetic field for two representative YAlO₃/KTaO₃ heterostructures (Samples #1 and #2). Low temperature-dependent R_s is illustrated in the inset of (a). Magnetoresistance for fields (b) parallel and (c) perpendicular to the Sample #1 plane surface. (d) Temperature dependence of the upper critical field $\mu_0 H_{c2}$.

ducible and reasonably consistent with previous electrical transport studies on EuO/KTaO₃ [11, 12] and LaAlO₃/KTaO₃ [11, 13]. As the temperature is further decreased, notably, the resistance R_s undergoes a narrow and sharp transition with a transition width of less than 0.5 K to a zero-resistance state, signaling the appearance of superconductivity at the interface of YAlO₃/KTaO₃. The superconducting critical temperature is $T_c = 1.86$ K and 0.92 K for Samples #1 and #2, respectively, as defined by where the resistance is at the midpoint of the normal electrical resistance at 5 K, $R_s(T_c) = 0.5 \times R_s(5 \text{ K})$.

To further reveal the superconducting behaviors in YAlO₃/KTaO₃, we measure the magnetoresistance $R_s(\mu_0 H)$ (here, μ_0 is the vacuum permeability) at various temperatures between 0.5 K and 5 K with fields parallel ($\mu_0 H_{\parallel}$) and perpendicular ($\mu_0 H_{\perp}$) to the Sample #1 plane surface, as shown in Fig. 2(b) and (c), respectively. The fundamental superconducting behavior is clearly resolved in that the magnetoresistance $R_s(\mu_0 H)$ varies differently with $\mu_0 H_{\parallel}$ and $\mu_0 H_{\perp}$, and both the superconducting critical fields $\mu_0 H_{c2}^{\parallel}$ and $\mu_0 H_{c2}^{\perp}$ parallelly shift to a lower value with increasing the magnetic field, where $\mu_0 H_{c2}$ are evaluated at the midpoints of the normal-state resistance at 5 K. These results provide an indication of a two-dimensional superconducting feature in YAlO₃/KTaO₃. The temperature-dependent upper critical fields $\mu_0 H_{c2}$ are shown in Fig. 2(d) and are well fitted by the phenomenological two-dimensional Ginzburg-Landau (G-L) model [19]: $\mu_0 H_{c2}^{\perp}(T) = \frac{\Phi_0}{2\pi\xi_G^2}(1 - \frac{T}{T_c})$

and $\mu_0 H_{c2}^{\parallel}(T) = \frac{\Phi_0 \sqrt{12}}{2\pi \xi_{GL} d_{SC}} \sqrt{1 - \frac{T}{T_c}}$, where Φ_0 , ξ_{GL} , and d_{SC} denote a flux quantum, the in-plane superconducting coherence length at $T = 0$ K, and the effective thickness of superconductivity, respectively. Using the extrapolated $\mu_0 H_{c2}^{\perp}(0) = 0.98$ T and $\mu_0 H_{c2}^{\parallel}(0) = 13.81$ T, we find $\xi_{GL} = 18.4$ nm and $d_{SC} = 4.5$ nm, where ξ_{GL} is significantly larger than d_{SC} , suggestive of a two-dimensional superconductivity nature. Additionally, the in-plane $\mu_0 H_{c2}^{\parallel}(0)$ is substantially larger than the Pauli-paramagnetic pair-breaking field $B_P \approx 3.46$ T based on the BCS theory in the weak-coupling limit [20, 21]. High values of $\mu_0 H_{c2}^{\parallel}(0)$ exceeding B_P can be realized in the presence of strong spin-orbit coupling owing to the elastic scattering resulted in suppression of the effect of spin paramagnetism. The violation of this paramagnetic limit is a common phenomenon in interface superconductors [11, 13, 22–25], especially when the superconducting layer thickness $d_{SC} < 20$ nm, however, the mechanism for realizing $\mu_0 H_{c2}^{\parallel}(0)$ value in excess of B_P remains an open question [11]. Furthermore, the thickness of superconducting layer in $\text{YAlO}_3/\text{KTaO}_3(111)$ is $d_{SC} = 4.5$ nm, which is the thinnest value recorded in the heterointerface superconductors thus far [11, 13, 22–26]. This result is expected from our intuition that the strong confinement potential induced by YAlO_3 significantly restricts the superconducting electrons in a thinner superconducting layer [17]. On the other hand, the out-of-plane polar angle (θ) dependent critical field H_{c2}^{θ} at 1.5 K is also determined to quantitatively verify the two-dimensional behavior in $\text{YAlO}_3/\text{KTaO}_3$, as shown in Fig. S3 [18]. The θ -dependent $\mu_0 H_{c2}^{\theta}$ are fitted with the two-dimensional Tinkham formula and the three-dimensional anisotropic G-L model, given by $\frac{H_{c2}^{\theta} |\cos \theta|}{H_{c2}^{\perp}} + \left(\frac{H_{c2}^{\theta} \sin \theta}{H_{c2}^{\parallel}} \right)^2 = 1$ and $\left(\frac{H_{c2}^{\theta} \cos \theta}{H_{c2}^{\perp}} \right)^2 + \left(\frac{H_{c2}^{\theta} \sin \theta}{H_{c2}^{\parallel}} \right)^2 = 1$, respectively [27, 28]. A cusp-like peak is clearly observed at $\theta = 90^\circ$ (see Fig. S3 [18]), which is well described by the two-dimensional Tinkham model, as frequently observed in interfacial superconductivity [5, 11, 29] and layered transition metal dichalcogenides [28, 30].

Since the superconductivity in $\text{YAlO}_3/\text{KTaO}_3$ is two-dimensional, the Berezinskii-Kosterlitz-Thouless (BKT) transition controls the establishment of superconducting phase coherence [31, 32]. Here, the BKT transition temperature defines the vortex unbinding transition and can be determined using current-voltage (I - V) measurements as a function of temperature T , shown in Fig. 3(a). Below T_c , we find a critical current I_c , whose value decreases with increasing measurement temperature. The maximal value of I_c is 330 A at 0.5 K, which is substantially higher than that observed in EuO/KTaO_3 [11] and $\text{LaAlO}_3/\text{KTaO}_3$ [13]. Such a high critical current value originates from the high charge carrier concentration of $1.45 \times 10^{14} \text{ cm}^{-2}$ confined in a thinner superconducting layer of $\text{YAlO}_3/\text{KTaO}_3$, promising for large-scale appli-

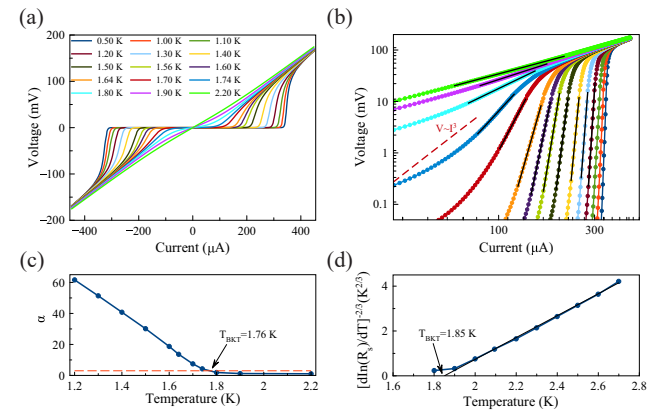


FIG. 3. (a) Temperature-dependent I - V measurements. (b) Corresponding logarithmic scale representation of (a). The long red dashed line denotes the $V \sim I^3$ dependence. (c) Temperature dependence of the power-law exponent α , as deduced from the fits shown in (b). (d) $R_s(T)$ dependence of the same sample, plotted on a $[d \ln(R_s)/dT]^{-2/3}$ scale.

cations in superconductor-based devices. In Fig. 3(b), we also plot I - V on a log-log scale and observe that the slope of the I - V characteristics smoothly evolves from the normal ohmic state, $V \propto I$, to a steeper power law resulting from the current exciting free-moving vortices, $V \propto I^{\alpha(T)}$, with $\alpha(T_{BKT}) = 3$. In Fig. 3(c), the T_{BKT} is interpolated to be 1.76 K, which is consistent with T_c as defined in Fig. 2(a). In addition, close to T_{BKT} , an $R_s = R_0 \exp[-b(T/T_{BKT} - 1)^{-1/2}]$ dependence, where R_0 and b are material parameters, is expected [33]. As shown in Fig. 3(d), the measured $R_s(T)$ is also consistent with this behavior and yields $T_{BKT} = 1.85$ K, in good agreement with the analysis of the α exponent.

Next, we discuss the in-plane anisotropy of superconductivity in $\text{YAlO}_3/\text{KTaO}_3$ using an in-plane azimuthal angle φ -dependent magnetoresistance, where φ is defined as the azimuthal angle between the magnetic field and the $[1\bar{1}0]$ -axis of the lattice, as indicated in Fig. 1(d). In the normal state [$T = 5$ K in Fig. 4(a)], the magnetoresistance R_s is found to be essentially independent of φ , displaying isotropic behavior. While in the superconducting state [$T = 1.5$ K in Fig. 4(a)], we observe a pronounced asymmetric twofold oscillations of the magnetoresistance R_s [see Fig. 4(b)]. In this case, the anisotropic magnetoresistance R_s attains the maximum value when the magnetic field is directed along the $[11\bar{2}]$ -axis ($\varphi = 90^\circ$) and becomes minimum when the field is directed along the $[1\bar{1}0]$ -axis ($\varphi = 0^\circ$) (also see Fig. S4 [18]). Considering that the existence of striking asymmetric twofold oscillations in magnetoresistance manifests deep inside the superconducting region and vanishes in the normal state, we can straightforwardly rule out the possibilities of extrinsic contributions, such as the magnetic field induced Lorentz force effect [34] and the electronic band structure inherent to the KTaO_3 with respect to the under-

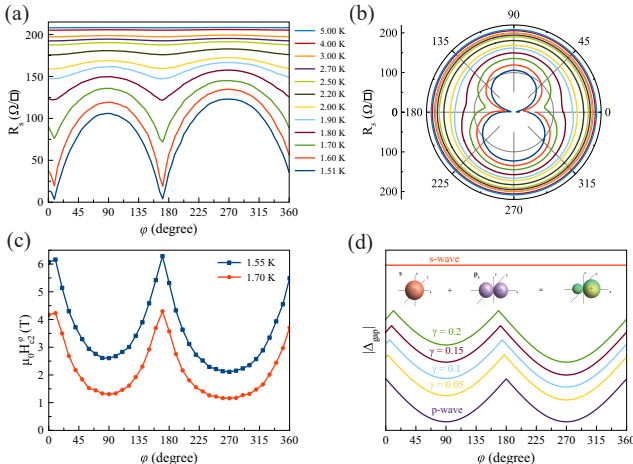


FIG. 4. (a) In-plane angular-dependent magnetoresistance R_s at various temperatures for an applied field of 3 T. (b) Polar plots of the data in (a). (c) In-plane angular-dependent $\mu_0H_{c2}^\varphi$ at various temperatures. (d) Theoretical evaluations of mixed-parity superconducting gap $|\Delta_{gap}|$ with mixture of s -wave Δ_s and p -wave Δ_p components. The ratio of Δ_s and Δ_p is denoted as γ . Schematic mixture of $s+p$ -wave pairing orbital symmetry is illustrated in the inset of (d).

lying threefold lattice symmetry [35] [also see Fig. 1(c)], and thus demonstrate that this anisotropy is an intrinsic property of the superconducting phase in $\text{YAlO}_3/\text{KTaO}_3$.

To further reveal the twofold asymmetric superconductivity in $\text{YAlO}_3/\text{KTaO}_3$ reflecting the superconducting gap structure, we extract the upper critical field μ_0H_{c2} from φ -dependent magnetoresistance R_s in the superconducting region. Interestingly, the in-plane φ -dependent $\mu_0H_{c2}^\varphi$ also displays asymmetric twofold oscillations, providing additional strong evidence for the twofold rotational asymmetry of the superconductivity in $\text{YAlO}_3/\text{KTaO}_3$. In addition, this oscillation of $\mu_0H_{c2}^\varphi$ has a π phase shift compared with that of the magnetoresistance R_s shown in Fig. 4(a) such that at the φ where superconductivity is hardest to suppress, $\mu_0H_{c2}^\varphi$ is largest and the magnetoresistance R_s is lowest [Fig. 4(a) and (c)], as expected from our intuitions [34, 36]. Since $\mu_0H_{c2}^\varphi$ takes maxima for the field applied parallel to the $[1\bar{1}0]$ -axis, and minima for the directions 90° from the $[1\bar{1}0]$ -axis, the superconducting gap leads to a maximum along the $[1\bar{1}0]$ -axis and a minimum along the $[1\bar{1}\bar{2}]$ -axis, whose topological contour is similar to that of sp -hybridization in molecule [37] [see the inset figure of Fig. 4(d)], signaling that the pairing symmetry of $\text{YAlO}_3/\text{KTaO}_3$ most likely belongs to the $s+p$ -wave.

Having experimentally established the asymmetric twofold anisotropy of the superconducting state of $\text{YAlO}_3/\text{KTaO}_3$, we proceed to elaborate on its origin of $s+p$ -wave pairing using the underlying symmetries of the crystal structure without requiring the details of the pairing mechanisms based on the group theoretical formulation of the Ginzburg-Landau theory [38], which al-

lows us to obtain the fundamental information about the superconducting ground state in $\text{YAlO}_3/\text{KTaO}_3$ superconductor. From the viewpoint of group symmetry, if a superconductor possesses an inversion symmetry, the Pauli principle requiring a totally antisymmetric Cooper pair wavefunction imposes the condition that the superconducting states should be either spin-singlet or spin-triplet, and the mixed-parity states are forbidden [38]. In the $\text{YAlO}_3/\text{KTaO}_3$ the lack of inversion symmetry, however, tends to mix spin-singlet and spin-triplet parts driven by strong spin-orbit coupling [39]. Indeed, the strong spin-orbit coupling with electrons originating from the heavy Ta 5d orbitals has been revealed at KTaO_3 interfaces [35, 40]. Due to the absence of mirror plane parallel to the interface of $\text{YAlO}_3/\text{KTaO}_3$, the point group of $\text{YAlO}_3/\text{KTaO}_3$ is C_{3v} , which does not contain the symmetry element of inversion. This situation is analogue to non-centrosymmetric superconductors [39]. Inspecting the character table of C_{3v} point group listed in Table S1 [18], we notice that the mixed-parity superconducting state only belongs to the $A1+E$ -representation with the possible basis function of $s+p$. Interestingly, the two-dimensional irreducible representation of E can spontaneously break the threefold rotational symmetry of the crystal [see Fig. 1(c)], leading to a subsidiary uniaxial anisotropy [41], such as a uniaxial p_x -wave or p_y -wave pairing. Since the upper critical field is proportional to the superconducting gap amplitude [42], $\mu_0H_{c2}^\varphi \propto |\Delta_{gap}(\varphi)|$, only the $s+p_x$ -wave pairing could give rise to an overall asymmetric twofold anisotropic gap shown in Fig. 4(c). In Fig. 4(d), we theoretically evaluate the mixed-parity superconducting gap $|\Delta_{gap}|$ as a function of the ratio of s -wave Δ_s and p -wave Δ_p components, $\gamma = \Delta_s/\Delta_p$. In the limit of s -wave and p -wave pairing, the $|\Delta_{gap}|$ exhibits isotropy and perfect twofold modulations, respectively. As increasing the ratio of γ from twofold p -wave modulations, the asymmetric anisotropy is gradually visible. The larger the ratio of γ reaches, the more significance the asymmetry will be. These theoretical results are in good agreement with the experimental observations shown in Fig. 4(c) (also see Fig. S5 [18]). Therefore, we attribute the KTaO_3 interface with inversion symmetry breaking to be an anisotropic mixed-parity superconductor with the mixture of s -wave and p -wave pairings, which realizes an appealing example followed the non-centrosymmetric bulk superconductors via heterostructure engineering, and opens a new platform to clarify the emergence of unconventional superconductivity with a delicate interplay of strong electron correlation and spin-orbit coupling inherent to the inversion symmetry breaking in the heterostructures.

Acknowledgments.—This work was supported by the National Natural Science Foundation of China (Grant Nos. 61871134 and 11927807) and Shanghai Science and Technology Committee (Grant Nos. 19ZR1402600 and 20DZ1100604). Y.S. also sponsored by Shanghai Pujiang

program (No. 20PJ1410900).

* G. Zhang, L. Wang, and J. Wang contributed equally to this work.

† E-mail: songyr@shanghaitech.edu.cn

‡ E-mail: lijun3@shanghaitech.edu.cn

§ E-mail: w_li@fudan.edu.cn

-
- [1] Y. Saito, T. Nojima, and Y. Iwasa, *Nature Reviews Materials* **2**, 16094 (2017).
- [2] J. Mannhart and D. G. Schlom, *Science* **327**, 1607 (2010).
- [3] P. Zubko, S. Gariglio, M. Gabay, P. Ghosez, and J.-M. Triscone, *Annu. Rev. Condens. Matter Phys.* **2**, 141 (2011).
- [4] H. Y. Hwang, Y. Iwasa, M. Kawasaki, B. Keimer, N. Nagaosa, and Y. Tokur, *Nature Materials* **11**, 103 (2012).
- [5] N. Reyren, Thiel, A. D. Caviglia, L. F. Kourkoutis, G. Hammerl, C. Richter, C. W. Schneider, T. Kopp, A.-S. Rüetschi, D. Jaccard, M. Gabay, D. A. Muller, J.-M. Triscone, J. Mannhart, *Science* **317**, 1196 (2007).
- [6] A. Gozar, G. Logvenov, L. Fitting Kourkoutis, A. T. Bollinger, L. A. Giannuzzi, D. A. Muller, and I. Bozovic, *Nature* **455**, 782 (2008).
- [7] Q.-Y. Wang, Z. Li, W.-H. Zhang, Z.-C. Zhang, J.-S. Zhang, W. Li, H. Ding, Y.-B. Ou, P. Deng, K. Chang, J. Wen, C.-L. Song, K. He, J.-F. Jia, S.-H. Ji, Y.-Y. Wang, L.-L. Wang, X. Chen, X.-C. Ma, and Q.-K. Xue, *Chin. Phys. Lett.* **29**, 037402 (2012).
- [8] J.-F. Ge, Z.-L. Liu, C. Liu, C.-L. Gao, D. Qian, Q.-K. Xue, Y. Liu, and J.-F. Jia, *Nature Materials* **14**, 285 (2015).
- [9] F.-C. Hsu, J.-Y. Luo, K.-W. Yeh, T.-K. Chen, T.-W. Huang, P. M. Wu, Y.-C. Lee, Y.-L. Huang, Y.-Y. Chu, D.-C. Yan, and M.-K. Wu, *Proc. Natl. Acad. Sci. U. S. A.* **105**, 14262 (2008).
- [10] J. J. Lee, F. T. Schmitt, R. G. Moore, S. Johnston, Y.-T. Cui, W. Li, M. Yi, Z. K. Liu, M. Hashimoto, Y. Zhang, D. H. Lu, T. P. Devereaux, D.-H. Lee, and Z.-X. Shen, *Nature* **515**, 245 (2014).
- [11] C. Liu, X. Yan, D. Jin, Y. Ma, H.-W. Hsiao, Y. Lin, T. M. Bretz-Sullivan, X. Zhou, J. Pearson, B. Fisher, J. S. Jiang, W. Han, J.-M. Zuo, J. Wen, D. D. Fong, J. Sun, H. Zhou, and A. Bhattacharya, *Science* **371**, 716 (2021).
- [12] Y. Ma, J. Niu, W. Xing, Y. Yao, R. Cai, J. Sun, X. C. Xie, X. Lin, and W. Han, *Chin. Phys. Lett.* **37**, 117401 (2020).
- [13] Z. Chen, Z. Liu, Y. Sun, X. Chen, Y. Liu, H. Zhang, H. Li, M. Zhang, S. Hong, T. Ren, C. Zhang, H. Tian, Y. Zhou, J. Sun, and Y. Xie, *Phys. Rev. Lett.* **126**, 026802 (2021).
- [14] K. Ueno, S. Nakamura, H. Shimotani, H. T. Yuan, N. Kimura, T. Nojima, H. Aoki, Y. Iwasa, and M. Kawasaki, *Nature Nanotechnology* **6**, 408 (2011).
- [15] P. Villar Arribi, A. Paramekanti, and M. R. Norman, *Phys. Rev. B* **103**, 035115 (2021).
- [16] A. Biswas, C.-H. Yang, R. Ramesh, and Y. H. Jeong, *Progress in Surface Science* **92**, 117 (2017).
- [17] Z. Chen, A. G. Swartz, H. Yoon, H. Inoue, T. A. Merz, D. Lu, Y. Xie, H. Yuan, Y. Hikita, S. Raghu, and H. Y.

Hwang, *Nature Communications* **9**, 4008 (2018).

- [18] See Supplemental Material for Materials and Methods, Figs. S1-S5, and Table S1.
- [19] M. Tinkham, *Introduction to Superconductivity*, 2nd edn (McGraw-Hill, New York, 1996).
- [20] B. S. Chandrasekhar, *Appl. Phys. Lett.* **1**, 7 (1962).
- [21] A. M. Clogston, *Phys. Rev. Lett.* **9**, 266 (1962).
- [22] M. Kim, Y. Kozuka, C. Bell, Y. Hikita, and H. Y. Hwang, *Phys. Rev. B* **86**, 085121 (2012).
- [23] N. Reyren, S. Gariglio, A. D. Caviglia, D. Jaccard, T. Schneider, and J.-M. Triscone, *Appl. Phys. Lett.* **94**, 112506 (2009).
- [24] Y.-L. Han, S.-C. Shen, J. You, H.-O. Li, Z.-Z. Luo, C.-J. Li, G.-L. Qu, C.-M. Xiong, R.-F. Dou, L. He, D. Naugle, G.-P. Guo, and J.-C. Nie, *Appl. Phys. Lett.* **105**, 192603 (2014).
- [25] A. M. R. V. L. Monteiro, D. J. Groenendijk, I. Groen, J. de Bruijckere, R. Gaudenzi, H. S. J. van der Zant, and A. D. Caviglia, *Phys. Rev. B* **96**, 020504(R) (2017).
- [26] J. Biscaras, N. Bergeal, A. Kushwaha, T. Wolf, A. Rastogi, R.C. Budhani, and J. Lesueur, *Nature Communications* **1**, 89 (2010).
- [27] M. Tinkham, *Phys. Rev.* **129**, 2413 (1963).
- [28] J. M. Lu, O. Zheliuk, I. Leermakers, N. F. Q. Yuan, U. Zeitler, K. T. Law, and J. T. Ye, *Science* **350**, 1353 (2015).
- [29] L. Wang, H. Xue, G. Zhang, Z. Shen, G. Mu, S. Wu, Z. An, Y. Chen, and W. Li, *arXiv:2106.06948* (2021).
- [30] D. Jiang, T. Yuan, Y. Wu, X. Wei, G. Mu, Z. An, and W. Li, *ACS Appl. Mater. Interfaces* **12**, 49252 (2020).
- [31] J. M. Kosterlitz and D. J. Thouless, *J. Phys. Chem.* **5**, L124 (1972).
- [32] M. R. Beasley, J. E. Mooij, and T. P. Orlando, *Phys. Rev. Lett.* **42**, 1165 (1979).
- [33] B. I. Halperin and D. R. Nelson, *J. Low Temp. Phys.* **36**, 599 (1979).
- [34] H. Xue, L. Wang, Z. Wang, G. Zhang, W. Peng, S. Wu, C. Gao, Z. An, Y. Chen, and W. Li, *arXiv:2110.13397* (2021).
- [35] F. Y. Bruno, S. M. Walker, S. Riccò, A. de la Torre, Z. Wang, A. Tamai, T. K. Kim, M. Hoesch, M. S. Bahramy, and F. Baumberger, *Adv. Electron. Mater.* **5**, 1800860 (2019).
- [36] A. Hamill, B. Heischmidt, E. Sohn, D. Shaffer, K.-T. Tsai, X. Zhang, X. Xi, A. Suslov, H. Berger, L. Forró, F. J. Burnell, J. Shan, K. F. Mak, R. M. Fernandes, K. Wang, and V. S. Pribiag, *Nature Physics* **17**, 949 (2021).
- [37] M. S. Dresselhaus, G. Dresselhaus, and A. Jorio, *Group Theory: Application to the physics of condensed matter*, (Springer, Berlin Heidelberg, 2008).
- [38] M. Sigrist and K. Ueda, *Rev. Mod. Phys.* **63**, 239 (1991).
- [39] E. Bauer and M. Sigrist, *M. Non-centrosymmetric superconductors: Introduction and overview*, (Springer, Berlin Heidelberg, 2012)
- [40] K. Rubi, S. Zeng, F. Bangma, M. Goiran, A. Ariando, W. Escoffier, and U. Zeitler, *Phys. Rev. Research* **3**, 033234 (2021).
- [41] S. Yonezawa, *Condens. Matter* **4**, 2 (2019).
- [42] J. D. Strand, D. J. Bahr, D. J. Van Harlingen, J. P. Davis, W. J. Gannon, and W. P. Halperin, *Science* **328**, 1368 (2010).